Impact of Dynamic Voltage Support on Memory Polarized Mho Relay in Presence of Grid Following PV Generators

Jayamohan, Meenu; Das, Sarasij; De Jesus Chavez, Jose; Popov, Marjan

DOI
10.1109/ISGTEUROPE62998.2024.10863631

Publication date
2024

Document Version
Final published version

Published in
IEEE PES Innovative Smart Grid Technologies Europe, ISGT EUROPE 2024

2024 IEEE PES Innovative Smart Grid Technologies Europe (ISGT EUROPE) | 979-8-3503-9042-1/24/$31.00 ©2024 IEEE | DOI: 10.1109/ISGTEUROPE62998.2024.10863631

Impact of Dynamic Voltage Support on Memory Polarized Mho Relay in Presence of Grid Following PV Generators

Meenu Jayamohan
Student Member, IEEE
Electrical Engineering
Indian Institute of Science
Bangalore, India
meenuj@iisc.ac.in

Sarasij Das
Senior Member, IEEE
Electrical Engineering
Indian Institute of Science
Bangalore, India
sarasij@iisc.ac.in

Jose de Jesus Chavez
Senior Member, IEEE
School of Engineering and Sciences
Tecnologico de Monterrey
Guadalajara, Mexico
j.j.chavezmuro@tec.mx

Marjan Popov
Fellow, IEEE
Faculty of EEMCS
Delft University of Technology
Delft, The Netherlands
M.Popov@tudelft.nl

***Abstract*—This paper investigates the influence of dynamic voltage support on Positive Sequence Memory-Polarized (PSMP) mho relays in the presence of Grid Following Photovoltaic (PV) generators. The widespread integration of Inverter-Based Resources (IBRs) has significantly altered power system dynamics. Traditionally, memory polarization in mho elements has ensured reliable operation during close-in faults. A dynamic expansion of mho characteristics results from the use of memory voltage for polarizing the mho elements, enhancing the resistive reach in systems dominated by Synchronous Generators (SGs). However, the fault current characteristics of IBRs differ from SGs, potentially compromising the dynamic mho expansion behavior. This work explores how dynamic voltage support employed by large-scale PV generators affects the expansion of PSMP mho characteristics. The PV generators used in this study have reactive power priority and Low Voltage Ride-Through /High Voltage Ride-Through capabilities and are compliant with the IEEE Standard 2800-2022.**

***Index Terms*—Dynamic mho expansion, K-factor, memory polarization, PV generator, reactive power support**

I. Introduction

The introduction of power electronic converters into the bulk power system has significantly altered the dynamics of the power system. Inverter-Based Resources (IBRs), like Wind Turbine Generators (WTGs) and Photovoltaic (PV) generators, are interfaced with the grid using power electronic converters. Grid Following (GFOL) converters are widely used in the existing power system where the voltage and frequency of the IBR system are dictated by the grid. To mitigate cascading outages and bolster grid resilience against disturbances, modern grid codes have transitioned from demanding fast tripping of IBRs during voltage dips to mandating Fault Ride-Through (FRT) [1]. The PV system should maintain the voltage at its terminals during FRT conditions by providing additional reactive power through dynamic voltage support along with dynamic reactive power support [1], [2]. The K-factor represents the additional reactive power support provided in proportion to the drop in voltage at the Reference Point of Applicability (RPA) [1]. IBR maintains voltage stability during grid faults by prioritizing reactive power, called Q-priority, potentially reducing active power output. However, existing grid codes lack specific requirements for active power injection during FRT events. The existing literature addresses the impact of dynamic voltage support on the stability of the system [2] - [5]. The impact of IBRs on distance relays has been analyzed in [6] - [8]. However, the impact of dynamic voltage support on dynamic mho expansion has not been studied yet. For an IBR-integrated system, there is a decrease in fault current, short circuit strength, and inertia due to the addition of power electronic components. This challenges the existing protection schemes designed for traditional SG-only systems, potentially compromising their sensitivity and speed when used in an IBR-integrated system.

Memory polarisation technique is employed in mho elements for transmission line protection to identify close-in faults [9]. The basic idea behind these memory polarization elements is that, in the event of a fault, only the voltage amplitude changes rapidly, with little changes to its phase angle and frequency. Also, it is predicated on the accurate estimation of the increased resistive reach due to the consistent and predictable source impedance amplitude behind the relay [9]. This applies to an SG-only system. For systems having IBRs, this assumption might not be true. The phase angle may deviate from its pre-fault value. References [10] and [11] analyze the impact of IBR on memory-polarized mho relay elements. A novel offset-mho characteristics for memory polarized relay has been developed in [12]. The impacts of $V_{dc}Q$ control-based PV generation on Positive Sequence Memory Polarized (PSMP) mho relays are presented in [13]. It has analyzed the PSMP mho element with respect to pre-fault steady state operating point, changing weights, and behavior of converter control. But, references [10] - [13] do not take into account the IEEE Standard 2800-2022 [1]. The benefits of the IEEE Standard 2800-2022 on various transmission line distance protection functions are discussed in detail in [13]. However, the existing literature, including [10] - [13], does not consider the impact of the K-factor on the dynamic mho expansion. This work presents the study of dynamic mho expansion for PSMP mho relays in a transmission system with GFOL PV generation. The major contributions of this work

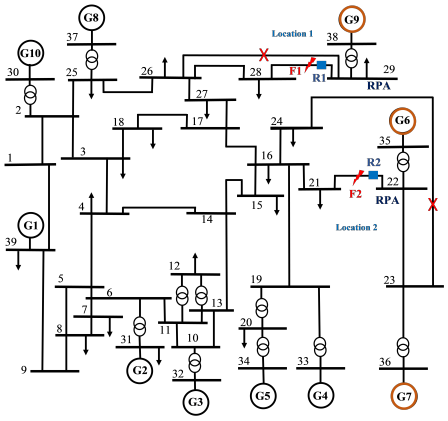

Fig. 1. Modified IEEE-39 bus system

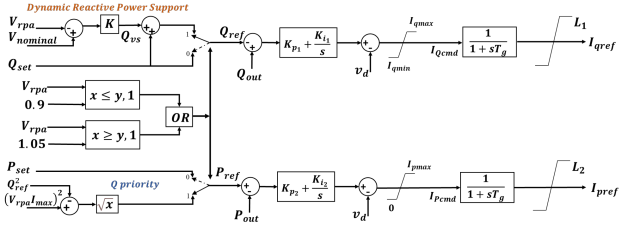

Fig. 2. Control logic for the GFOL PV generator

are presented below.

- The dynamic mho expansion of PSMP mho relay has been studied by varying the K-factor. Two different relay locations are considered, where the fault current seen by the relays, $R1$ and $R2$, are fully contributed by the PV generators.
- The dynamic mho expansion of PSMP mho relay has also been studied for two reactive power set points, corresponding to power factors 0.95 and 0.975 lag.
- By varying the K-factor, the diameter of the dynamic PSMP mho element's maximum expansion, d_{max}, and the angle of the memory vector, θ_m, have been examined.

II. System Configuration

The IEEE 39 bus system of 345 kV and 60 Hz is modified and modeled in PSCAD such that the relays see the fault current fully contributed by the PV generators as in Fig. 1. $R1$ and $R2$ show the two different relay locations, details of which are presented in Section IV. The Q-priority control scheme for the GFOL PV generator is shown in Fig. 2 [15]. This study presents a phasor domain analysis where the 60 Hz fundamental frequency phasor seen by the relay is analyzed. The switching-frequency dynamics are disregarded since the harmonic performance close to switching frequencies is not the objective of this study. Hence, the PV is modeled using an average model [16], [17]. A Synchronous Reference Frame PLL with a Low Pass Filter (LSRF PLL) is used. The PV inverter has Low Voltage Ride-Through (LVRT) and High Voltage Ride-Through (HVRT) capability, as presented in Fig. 3, implemented using dynamic voltage support [1].

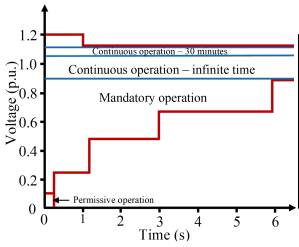

Voltage at RPA (p.u.)	Operating mode/response	Minimum ride-through time (s)
V>1.2	May ride-through / trip	NA
V>1.1	Mandatory operation	1
V>1.05	Continuous operation	1800
V<0.9	Mandatory operation	6
V<0.7	Mandatory operation	3
V<0.5	Mandatory operation	1.2
V<0.25	Mandatory operation	0.32
V<0.1	Permissive operation	0.32

Fig. 3. Low Voltage/High Voltage Ride-Through characteristics

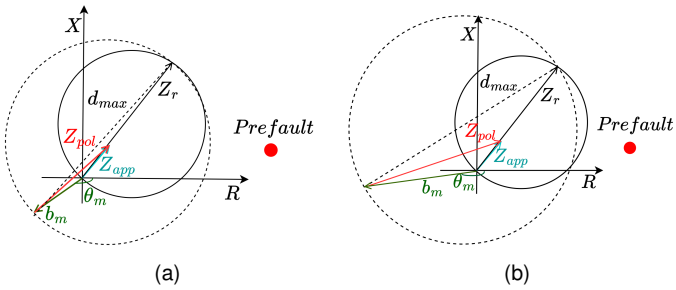

Fig. 4. Dynamic mho expansion for (a) SG-only system (b) system with PV integration

Throughout the paper, constant solar irradiation and temperature are assumed.

At RPA, under steady-state operating conditions, the voltage will remain between 0.9 p.u. and 1.05 p.u. [1]. Under steady-state conditions, the Maximum Power Point Tracker (MPPT) output, P_{set}, is considered as P_{ref}, and Q_{ref} is set as Q_{set}. The constant values of the Proportional-Integral (PI) blocks used in the PV control are K_{p1}=K_{p2}=0.05 and K_{i1}=K_{i2}=1 and T_g=0.02 s. When activated, the voltage support functionality offers reactive power support as per the grid code. When the voltage is out of the limits, (1)-(3) are used to calculate the real and reactive power reference values. The voltage support feature provides additional reactive power, Q_{vs}, in proportion to the change in voltage at RPA (V_{rpa}) relative to the nominal value ($V_{nominal}$) using the K-factor [1].

$$Q_{vs} = K(V_{nominal} - V_{rpa}) \tag{1}$$

K (K-factor) can range from 1 to 10 [15]. When voltage support gets activated in the Q-priority mode,

$$Q_{ref} = Q_{vs} + Q_{set} \tag{2}$$

$$P_{ref} = \sqrt{(V_{rpa} I_{max})^2 - Q_{ref}^2} \tag{3}$$

where, to restrict the inverter's output current, I_{max} is set to 1.2 p.u.. All quantities in the above equations are in per unit.

III. Dynamic Mho Characteristics

For a mho relay element, Z_{pol} and Z_{op} are the polarizing and operating quantities, respectively. Here, the impedance of the protected portion of the transmission line, Z_r, is the reach setting of the relay. The apparent impedance seen by the relay is Z_{app}. This is calculated by the mho element from the voltages and currents of the system. The operating

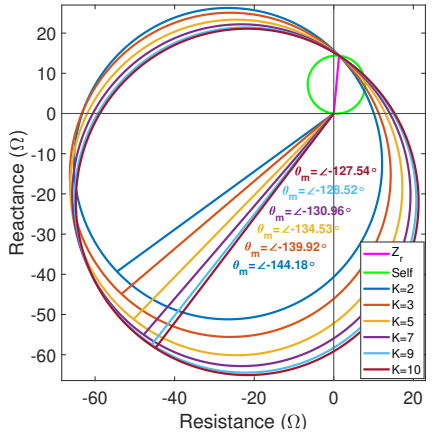

Fig. 5. Maximum dynamic mho expansion seen by relay $R1$ when K-factor is varied for 0.95 pf lag

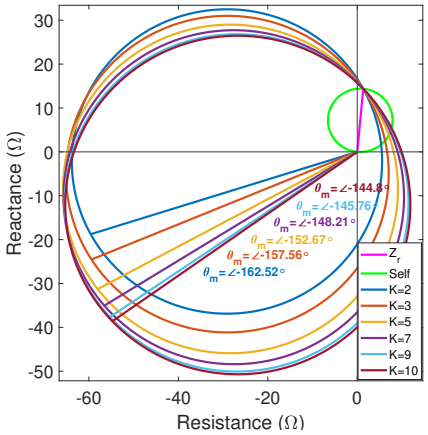

Fig. 6. Maximum dynamic mho expansion seen by relay $R1$ when K-factor is varied for 0.975 pf lag

quantity, Z_{op}, of the mho element is Z_{op}= Z_r-Z_{pol}. The self-polarized mho element is detailed in [9], [12]. The limitations of self-polarized mho relays during close-in faults led to the development of memory polarization techniques.

The polarizing quantity in the voltage plane for the self-polarized mho element is the faulted phase voltage. This faulted phase voltage may not be sufficient to polarize the mho relay element during a close-in fault, as the voltage will be near zero or zero. Hence, memory polarization is used to increase the reliability of the mho element. A PSMP mho relay is widely used for transmission line protection. It uses positive sequence pre-fault voltage as the polarizing quantity instead of the faulted voltage. The pre-fault voltage will be around the nominal value even during the fault, which will be sufficient to polarize the mho relay element during close-in faults, unlike the self-polarized mho element. The phrase "memory voltage" refers to this pre-fault voltage. A memory filter produces the memory voltage, and over time, it converges progressively to the fault voltage itself. In a PSMP mho relay, the Z_{pol} will be calculated from the fault current, I_f, and positive sequence memory voltage, $V^+_{f,m}$. For the i^{th} protection pass, the memory voltage is defined as,

$$V^+_{f,m}(i) = \omega.V^+_f(i) + (1-\omega).V^+_{f,m}(i-j) \tag{4}$$

where $V^+_{f,m}$ is the positive sequence memory voltage phasor, V^+_f is the positive sequence faulted phase voltage phasor, and ω is the weight factor which can have values between 0 and 1. In this study, ω is set as 0.5. Voltage belonging to $i-j$ protection pass is used as memory voltage for the i^{th} protection pass. This polarizing memory voltage will cause dynamic mho expansion. The dynamic PSMP mho expansion for a three-phase to ground fault for an SG-only system is shown in Fig. 4a. The vector b_m denotes the memory vector, and θ_m denotes the angle of the memory vector from the positive resistance axis (R-axis). The apparent impedance, Z_{app}, and the polarizing impedance, Z_{pol} for a three-phase to ground fault are calculated as,

$$Z_{app}(i) = \frac{V_f(i)}{I_f(i)}; \qquad Z_{pol}(i) = \frac{V^+_{f,m}(i)}{I_f(i)} \tag{5}$$

The memory vector, b_m, and the diameter of the dynamic mho circle, d_m are calculated as

$$b_m(i) = Z_{app}(i) - Z_{pol}(i); \quad d_m(i) = |Z_r(i) - b_m(i)| \tag{6}$$

The maximum value of $d_m(i)$ is represented as d_{max}, which is the maximum dynamic PSMP mho expansion. The corresponding angle of b_m with the positive R-axis at d_{max} is represented as θ_m. The dynamic expansion of the mho circle is governed by b_m. This dynamic expansion has been found to provide more resistive coverage for the mho element. In Fig. 4a, the magnitude of Z_{pol} is low for an SG-only system due to low pre-fault voltage and high fault current. This, in turn, makes b_m small, which is a resultant of Z_{pol} and Z_{app}. However, from Fig. 4b for PV-integrated system, it can be seen that the b_m is much longer, and its angle, θ_m, is higher than that for SG-only system, which reduces its resistive reach [9]. Henceforth, within this work, a higher value of θ_m signifies that the memory vector b_m is moving away from the positive R-axis or negative X-axis and vice-versa.

IV. Results

The results are obtained using a sampling rate of 3.84 kHz to acquire 64 samples/cycle. The fault data extracted from the simulation has been used to do post-processing calculations. Eight protection passes are considered in a cycle. The prior two cycle's memory voltage is obtained by setting the value j in (4) to 16. The maximum expansion of the dynamic mho characteristic of the PSMP mho element in a PV-integrated system by varying the K-factor along with self-polarized mho characteristics are presented. An analysis is conducted on trends found in the diameter of the maximum expansion of the dynamic PSMP mho circle, d_{max}, and the memory voltage angle θ_m, made during maximum expansion, by varying the K-factor corresponding to the dynamic voltage support. The K-factor is varied from 2 to 10.

A. *Location* 1- *Relay* $R1$

In this case, G9 connected to Bus 38 is replaced with an 870.5 MVA, 33 kV GFOL PV generator. The line 26-29 is

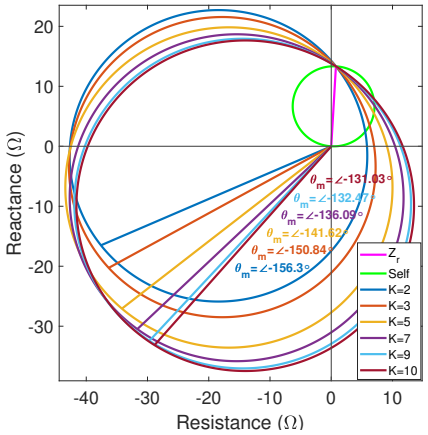

Fig. 7. Maximum dynamic mho expansion seen by relay $R2$ when K-factor is varied for 0.95 pf lag

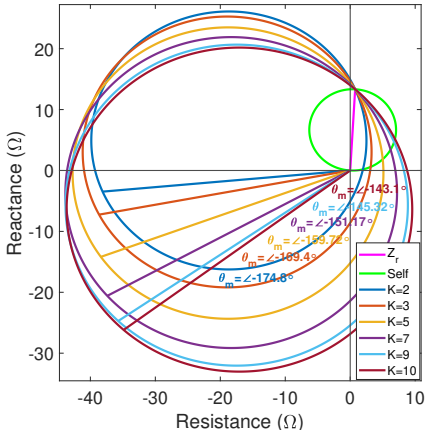

Fig. 8. Maximum dynamic mho expansion seen by relay $R2$ when K-factor is varied for 0.975 pf lag

removed, and load flow is performed for the modified system. This ensures that the fault current seen by relay $R1$ is fully contributed by the PV generator (see Fig. 1). A three-phase to ground fault, $F1$, is generated on line 28–29 for a time of 0.07 s at a distance of 2% from relay $R1$. The results are presented for fault resistance R_f = 0 Ω.

1) Case: Q_{set}=0.3287P_{set} (0.95 pf): Here, the steady state reactive power set point Q_{set} of the PV generators is set as 0.3287 times their active power set point, P_{set}, for the default MVA rating. This corresponds to a steady-state power factor (pf) of 0.95. It has been observed that, with the increase in K-factor, the d_{max} increases and corresponding θ_m decreases. This implies that there is an improvement in the resistive reach during dynamic expansion when the K-factor increases. It has also been observed that the change in d_{max} is significant for lower K values of 2 and 3, while the change in d_{max} becomes negligible around higher K values of 9 and 10. A similar trend is observed for the change in θ_m when the K-factor is varied. This is shown in Fig. 5.

2) Case: Q_{set}=0.2279P_{set} (0.975 pf): Here, the steady state reactive power set point Q_{set} of the PV generators is set as 0.2279 times their active power set point, P_{set}, for the default MVA rating. This corresponds to a steady-state power factor of 0.975. In this case, the K-factor is varied from 2 to 10. It has been observed that, with the increase in K-factor, the d_{max} increases and corresponding θ_m decreases, increasing the resistive reach during dynamic expansion with the increase in K-factor. The trend observed is the same as that observed in the previous case. It has also been observed that the increase in d_{max} and the decrease in θ_m are more significant in the lower K values while it becomes less significant at the higher K values. A similar trend is observed for the change in θ_m also when the K-factor is varied. This is shown in Fig. 6. However, for each K-factor (from 2 to 10), the d_{max} observed at 0.975 pf is consistently lower compared to that at 0.95 pf. Moreover, the θ_m corresponding to the d_{max} for 0.975 pf is higher than that for 0.95 pf. This larger angle for 0.975 pf positions the memory vector further away from the positive R-axis, consequently leading to an even greater reduction in the resistive reach.

B. Location 2- Relay $R2$

In this case, G6 and G7 are replaced with 683.27 MVA and 728.81 MVA GFOL PV generators, respectively. The line 23-24 is removed, and load flow is performed for the modified system. This ensures that the fault current seen by relay $R2$ is fully contributed by the PV generators. As shown in Fig. 1, a three-phase to ground fault, $F2$, is generated on line 21–22 for a time of 0.07 s at a distance of 2% from relay $R2$. The observations are presented for fault resistance R_f = 0 Ω.

The study is performed for Location 2 with steady-state power factor 0.975 and 0.95. The results for both the power factor cases show similar trends as in Location 1. With the increase in the K-factor, the d_{max} increases and θ_m decreases. Hence, there is a reduction in resistive reach during dynamic mho expansion at lower K values. Additionally, it has also been observed that the increase in d_{max} and the decrease in θ_m are more significant in the lower K values while it becomes less significant at the higher K values. Fig. 7 and Fig. 8 present the dynamic mho expansion for relay $R2$ when the steady-state power factor is 0.95 and 0.975, respectively.

C. Analysis of Observations

During a fault, the K-factor indicates the amount of additional reactive power to be injected to bring the voltage at the PV terminals to an acceptable value, as shown in (1). A high K-factor injects more reactive power than a low K-factor. As a result, with a higher K-factor, the reactive component of the impedance seen by the relay will be higher. This results in the memory vector being closer to the negative X-axis during maximum dynamic mho expansion. Hence, corresponding θ_m will be lower for a higher K-factor. A higher Q_{set} of 0.3287P_{set} corresponds to a lower steady-state power factor of 0.95, and a lower Q_{set} of 0.2279P_{set} corresponds to a higher steady-state power factor of 0.975. It has been observed from the results that a lower Q_{set} corresponds to a lower d_max during dynamic mho expansion and a higher θ_m from the positive R-axis. Hence, a lower Q_{set} results in a lower reactive

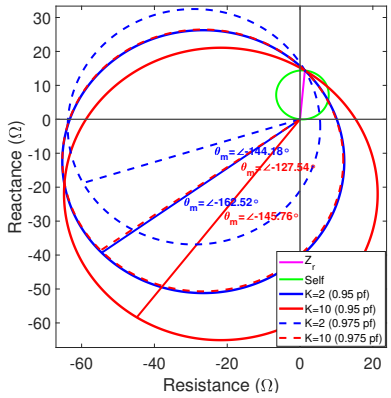

Fig. 9. Comparison of maximum dynamic mho expansion seen by relay $R1$ for $0.95\ pf$ lag and $0.975\ pf$ lag

component in the impedance seen by the relay, which results in the memory vector being far from the positive R-axis or negative X-axis. Hence, the resistive reach reduces for lower Q_{set} for corresponding K-factors compared to higher Q_{set}, as shown in Fig. 9.

D. Observations and Recommendation

- For a fixed steady-state power factor, the d_{max} increases and θ_m decreases (towards positive R-axis) as K-factor increases from 2 to 10.
- It has been observed that the change in d_{max} and θ_m are more significant at the lower K-factors and it becomes less significant around higher K-factors (9 and 10).
- For a fixed K-factor, the d_{max} is higher, and θ_m is lower for higher steady state reactive power reference/lower power factor for a fixed MVA rating.
- For some K values, the resistive reach of the PSMP mho relay gets reduced during dynamic expansion. Hence, it is recommended that the impact of the chosen K-factor should be thoroughly studied.

V. Conclusion

The impact of K-factor on the dynamic mho expansion of a PSMP mho relay for a system with large-scale PV integration has been presented in this paper. The maximum expansion of the dynamic mho circle, d_{max}, and the corresponding angle made by the memory vector, θ_m, are analyzed for different K-factors. It has been observed that the dynamic mho expansion of the PSMP mho relay depends on the K-factor used. The d_{max} increases while the θ_m decreases (towards positive R-axis) with the increase in the K-factor. This implies that the mho circle widens and slants towards the right due to the increase in the reactive component of the impedance seen by the relay as the K-factor increases. This results in a reduced resistive reach at lower K-factors and an improved resistive reach at higher K-factors. The results have been verified for two different locations where the entire fault current seen by the relay is contributed by the PV generator. Hence, the impact of the chosen K-factor for a system should be thoroughly examined in the context of memory-polarization.

Acknowledgment

This research has been partly performed using the ERIGrid 2.0 Research Infrastructure and is part of a project that has received funding from the European Union's Horizon 2020 Research and Innovation Programme under Grant Agreement No. 870620, to conduct research at Delft University of Technology, the Netherlands. This work has also been partly funded by the IISc-TU Delft Joint Seed Fund 2022.

References

[1] "IEEE Standard for Interconnection and Interoperability of Inverter-Based Resources (IBRs) Interconnecting with Associated Transmission Electric Power Systems," in IEEE Std 2800-2022, vol., no., pp.1-180, 22 April 2022.

[2] Y. Guo, B. C. Pal, R. A. Jabr and H. Geng, "Global Optimality of Inverter Dynamic Voltage Support," *IEEE Trans. Power Syst.*, vol. 37, no. 5, pp. 3947-3957, Sept. 2022.

[3] B. Weise, "Impact of K-factor and Active Current Reduction during Fault-Ride-Through of Generating Units Connected via Voltage-Sourced Converters on Power System Stability, " *IET Renew. Power Gener.*, 9(1):25–36, 2015.

[4] X. Zhang, M. Radwan, and S. Pirooz Azad, "Modified Distance Protection of Transmission Lines Originating from DFIG-Based WPPs by Considering the Impact of Fault-Induced Rotor Frequency and LVRT Requirements," *Int. J. Electr. Power Energy Syst.*, Vol. 147, 2023.

[5] G. Lammert et al., "Impact of Fault Ride-Through and Dynamic Reactive Power Support of Photovoltaic Systems on Short-Term Voltage Stability," 2017 IEEE Manchester PowerTech, UK, 2017, pp. 1-6.

[6] S. Paladhi and A. K. Pradhan, "Adaptive Distance Protection for Lines Connecting Converter-Interfaced Renewable Plants," *IEEE J. Emerg. Selec. Topics Power Electron.*, vol. 9, no. 6, pp. 7088–7098, Dec. 2021.

[7] J. J. Chavez, M. Popov, D. López, S.Azizi, and V. Terzija, "S-Transform based Fault Detection Algorithm for Enhancing Distance Protection Performance," *Int. J. Electr. Power Energy Syst.*, Vol. 130, 2021.

[8] B. Kasztenny, "Distance Elements for Line Protection Applications Near Unconventional Sources.", SEL Inc., Nov. 2022

[9] D. D. Fentie, "Understanding the Dynamic Mho Distance Characteristic," in 2016 69th Annual Conference for Protective Relay Engineers (CPRE), IEEE, 2016, pp. 1–15.

[10] M. J. B. B. Davi, M. Oleskovicz, F. V. Lopes, et al., "A Case Study-Based Review of the Impacts of Inverter-Interfaced Wind Power Plants on Distance Protections," *J. Control. Autom. Electr. Syst. 34*, 2023.

[11] A. Haddadi, M. Zhao, I. Kocar, E. Farantatos, and F. Martinez, "Impact of Inverter-Based Resources on Memory-Polarized Distance and Directional Protective Relay Elements," 2021 52nd North American Power Symposium (NAPS), Tempe, AZ, USA, 2021.

[12] E. Sorrentino, J. Melián, and V. De Andrade, "A Novel Method to Obtain the Offset Mho Characteristic of Memory-Polarized and Cross-Polarized Distance Functions of Protective Relays from Experimental Measurements," *Electric Power Syst. Res.*, Vol. 216, 2023.

[13] A. Radhakrishnan, A. Ghosh, I. R. Sai Priyamvada and S. Das, "Performance of Memory-Polarized Distance Relay in Presence of PV Generator with VdC-Q Control," IEEE Energy Conversion Congress and Exposition (ECCE), Detroit, MI, USA, 2022, pp. 1-8.

[14] M. J. B. B. Davi, M. Oleskovicz, F. V. Lopes, " Study on IEEE 2800-2022 Standard Benefits for Transmission Line Protection in the Presence of Inverter-Based Resources," *Electric Power Syst. Res.*, Vol. 220, 2023.

[15] M. Jayamohan, S. Das and S. Brahma, "Impedance Trajectories during Stable and Unstable Power Swings in Presence of PQ Control based PV Generations," 2023 IEEE PES General Meeting (PESGM), Orlando, FL, USA, Jul. 2023, pp. 1-5.

[16] U. Karaagac et al., "A Generic EMT-Type Model for Wind Parks With Permanent Magnet Synchronous Generator Full Size Converter Wind Turbines," *IEEE Power Energy Technol. Syst. J.*, vol. 6, no. 3, pp. 131-141, Sept. 2019.

[17] R. T. Elliott, A. Ellis, P. Pourbeik, J. J. Sanchez-Gasca, J. Senthil and J. Weber, "Generic Photovoltaic System Models for WECC - A Status Report," 2015 IEEE PES General Meeting (PESGM), Denver, CO, USA, Jul. 2015, pp. 1–5.